JOURNAL OF PROPULSION AND POWER
Vol. 27, No. 1, January–February 2011

Effect of Swirl on Mixing in Underexpanded Supersonic Airflow

A. Abdelhafez* and A. K. Gupta†
University of Maryland, College Park, Maryland 20742

DOI: 10.2514/1.48335

This study examines the effect of imparting swirl to underexpanded nozzle airflow on supersonic mixing under matched mass flow conditions. A convergent nozzle with swirling capabilities is used to generate the underexpanded airflow. Fuel is injected coaxially at the nozzle throat. Nonreacting conditions are considered, wherein fuel is simulated by mixtures of helium, argon, and krypton inert gases. It was found that the positive effect of swirl on supersonic mixing is noticeable, even at the low degree of swirl examined here. Better mixing was observed between the supersonic and subsonic parts of the diamond-shock air flowfield at no fuel injection as well as between the supersonic air and the subsonic injected fuel. The compressible mixing-layer thickness was found to increase slightly with swirl. However, when normalized to its incompressible counterpart, the compressible thickness was observed to decrease with swirl, because the former increases more with swirl than the latter. Decreasing the air–fuel relative Mach number and/or density ratio was found to deteriorate mixing. On the other hand, decreasing the compressibility of the injected fuel (i.e., injecting fuel at lower subsonic Mach numbers) improves mixing.

Nomenclature

a	=	speed of sound
D	=	nozzle-exit diameter (11 mm)
DR	=	air–fuel density ratio at injection plane
M_{rel}	=	air–fuel relative Mach number at injection plane
S	=	swirl number
v	=	velocity
x	=	fuel-mixture fraction
z	=	axial coordinate

Subscripts

a	=	axial
t	=	tangential

I. Introduction

SWIRLING flow in nozzles occurs in a number of important propulsion applications, including turbofans and turbojet engines, spin-stabilized rockets, and integral rocket/ramjets. In the first two cases, the tangential-velocity component is induced by the motion of turbine blades and by the rocket spin, respectively. For ramjets, experimental studies [1] have demonstrated that swirl generated by fixed vanes located in the dump combustor inlet can lead to significantly improved combustor performance. Clearly, the generated swirl in each of those propulsion systems will persist at some level to the inlet of exhaust nozzle. Therefore, it is important to examine the effect of the tangential-velocity component on nozzle flowfield so that design parameters, such as thrust and mass flow rate, can be accurately determined.

Research on subsonic swirling flows is abundant in the literature; however, little of a fundamental nature is known about supersonic swirling ones. Imparting swirl to fuel jets injected in supersonic airflow was shown in numerous studies to enhance mixing, especially in the near-field downstream of injection. Therefore, to counter the adverse effects of compressibility, adding swirl is advantageous for mixing. Swithenbank and Chigier [2] proposed in an early study that swirl-based injection might be useful in scramjet flowfields. Substantial increases in mixing rates between injected fuel and airstream are assumed to occur due to the creation of radial and axial pressure gradients in the swirling flow. It was further proposed that injectors with variable swirl could be fitted into scramjet combustion chambers. The rate of mixing, angle of jet expansion, and the size of internal reverse flow region could be controlled by changing the amount of swirl.

In a more recent study, Cutler and Doerner [3] experimentally investigated the effects of swirl and skew on the mixing of a light supersonic gas jet injected from a flat wall into a Mach 2.0 airstream. The direction of a jet injected from a wall orifice into the main flow is defined by the pitch and skew angles. The pitch angle is the angle between the injection velocity vector and its projection on the wall that hosts the orifice. The skew angle, on the other hand, is the angle between that projection and the local velocity vector of main flow. By definition, the skew angle lies within the wall plane and is measured from the local velocity vector of main flow. The sign convention of the skew angle is purely arbitrary. The tests of Cutler and Doerner were conducted at nominally equal injectant mass flow rate and total pressure, as well as exit static pressure of the injector nozzle. They concluded that the effect of combined swirl and skew on injectant mixing is to slightly increase mixing in the near field of the injection. Kraus [4] and Kraus and Cutler [5] conducted an experimental study to determine whether the addition of swirl improves the mixing of a supersonic jet of fuel simulant (helium or air) injected at 30° to the wall into a confined Mach 2.0 airflow. Their results showed that plumes from swirling and nonswirling jets had comparable penetration and area, but the swirling ones contained substantially less mass flow, which suggests better mixing efficiency.

Cutler et al. [6] proposed the addition of swirl to supersonic scramjet fuel jets as a method of enhancing fuel mixing. Enhanced mixing and flow recirculation were observed with the application of swirl, which was attributed to vortex breakdown. Yamasaki et al. [7] experimentally studied the effects of inlet swirl on the performance of a disk magnetohydrodynamic (MHD) generator. Their experiments were carried out using a novel disk MHD generator with 24 swirl vanes installed in a large shock-tube-driven facility. Remarkable improvements in both adiabatic and electrical efficiencies were observed by the introduction of inlet swirl.

Kitamura et al. [8] conducted particle image velocimetry (PIV) measurements to investigate the effect of applying swirl to the supersonic fuel jets on air–fuel mixing in scramjet combustors. Their experimental data showed that application of swirl results in significant mixing enhancement. In a similar investigation, Yaguchi

Received 30 November 2009; revision received 27 September 2010; accepted for publication 1 October 2010.

*Graduate Student, Department of Mechanical Engineering, 2181 Glenn Martin Hall. Student Member AIAA.

†Distinguished University Professor, Department of Mechanical Engineering, 2181 Glenn Martin Hall. Fellow AIAA.

et al. [9] used PIV to study the effect of swirl on mixing in supersonic jets. Multiple swirl strengths were considered. Planar velocity distributions of single and twin supersonic jets were determined by PIV, with emphasis on maximum velocity decay and half-width spread. The researchers concluded that application of swirl promotes mixing.

Vortex enhancement of supersonic mixing was studied experimentally by Settles [10]. Swirl was used to enhance shear layer growth and mixing. It was concluded that swirl enhances compressible mixing; the degree of enhancement increased with increase in swirl. Settles also reported that the effects of convective Mach number and density ratio (DR) on the enhancement effect of swirl are still unknown; thus, the effects were recommended for future work.

In another experimental study by Naughton et al. [11], compressible jets with various amounts of swirl and compressibility were optically interrogated using laser Doppler velocimetry and planar light scattering to obtain the mixing-layer growth rate. Swirling supersonic gas flow (He, N_2, and air) was injected in coflowing supersonic (Mach = 1.5–4.0) airflow. Different degrees of swirl were imparted to the injected gas by means of different sets of swirl vanes preceding a convergent–divergent nozzle. The swirl vane sets were designed to produce a free-vortex tangential-velocity profile at the vane exit with maximum angles of 15, 30, 45, and 60°. The C–D nozzles were designed using the method of characteristics for a fixed 1.4 ratio of specific heats and nominal Mach numbers (presumably nonswirling) of 2.5, 3.0, 3.5, and 4.0. The researchers concluded that the addition of swirl increases entrainment by up to 60% compared with a corresponding nonswirling case. The swirl-induced mixing enhancement was linked to a modification of the turbulence in the mixing layers surrounding the swirling jets. A parameter β was proposed to correlate the observed swirl-induced growth-rate enhancement. This parameter was derived assuming that the streamwise vorticity, generated in the mixing layer by the addition of small amounts of swirl, causes additional turbulent mixing that counters the adverse effects of compressibility and increases the growth rate. It was found that the growth-rate data for swirling jets collapse to a single curve when plotted against this parameter. Increased enhancement of the growth rate was predicted for higher values of β, which implies that the positive effect of swirl actually increases with compressibility, although the observed dimensional growth rates for the examined compressible swirling cases were still less than those of their incompressible counterparts. These findings agree strongly with those of the current study (as will be seen later) and of Abdelhafez and Gupta [12], where it was reported that the pitot thickness of the compressible shear layer increases with the application of swirl. However, when normalized to its incompressible counterpart, the compressible thickness was observed to decrease with swirl, because the former was found to increase more with swirl than the latter.

Murakami and Papamoschou [13] examined flow structure and mixing enhancement in two-dimensional (2-D) and axisymmetric supersonic jets surrounded by secondary annular subsonic coaxial ones. The supersonic jets were issued from a convergent–divergent nozzle operated at offdesign conditions. It was shown that the mixing enhancement using secondary parallel injection (referred to as MESPI by the researchers) halves the length of potential core in both axisymmetric and 2-D jets. A short distance past the potential core, mixing enhancement caused a reduction in the centerline Mach number of 30% in round jets and 20% in 2-D ones. The corresponding reduction in peak molar concentration of a scalar injected in the primary flow was 65% in round jets and around 40% in 2-D ones.

Carpenter [14] developed a linearized theory for underexpanded inviscid supersonic jets with arbitrary initial swirl. Estimates were made of the effect of swirl on the total radiated sound power of shock-associated noise. It was found that this noise can be greatly reduced, or even eliminated, at sufficiently high swirl levels, which can be achieved at the expense of a very small thrust loss. Noise elimination was believed to be due to enhanced mixing that leads to the disappearance of some initial shock cells.

In another study more pertinent to mixing in free supersonic flows, Yu et al. [15] experimentally examined mode-switching phenomena of supersonic jets with swirl. They observed that the shock-cell spacing of swirling jets is smaller than that of nonswirling ones, which suggests enhanced mixing. In nonswirling compressible jets, the typical 2-D vortex roll up is believed to be suppressed, and mixing and entrainment are reduced, as compared with incompressible jets. Therefore, to counter the adverse effects of compressibility on mixing, adding swirl to a supersonic jet is favorable. The enhanced entrainment and mixing in swirling supersonic jets is thought to be due to the inherent three-dimensionality associated with the axial component of turbulent vorticity in swirling jets. Yu [16] studied underexpanded supersonic jets to determine the effect of swirl on mixing efficiency. The screech tones, which result from the interaction of shock waves with unstable jet boundaries, were examined at different degrees of swirl for their effect on mixing. Implication of enhanced mixing was discussed. It was also reported that swirl did not eliminate shock cells, nor did it affect their quasi-periodic nature, in spite of the generation of a recirculation zone in strongly swirling jets.

In this paper, the effect of imparting swirl to underexpanded nozzle airflow on supersonic mixing is examined both experimentally and numerically. A condensate-seeded Mie-scattering technique is presented that allows for highlighting mixedness variation nonintrusively throughout the supersonic flowfield. Matched mass flow conditions are considered here. A convergent nozzle with swirling capabilities is used to generate the underexpanded airflow. Fuel is injected coaxially at the nozzle throat. Nonreacting conditions are considered, wherein fuel is simulated by mixtures of helium, argon, and krypton inert gases. Analyses are made of the effects of relative Mach number and DR across the air–fuel shear layer. The effects of these parameters on supersonic mixing are investigated under both nonswirling and swirling flow conditions.

II. Experimental Setup

The experimental investigation of this study has been performed at the University of Maryland supersonic facility. The used supersonic-nozzle assembly is shown schematically in Fig. 1. A convergent nozzle of inlet-to-exit area ratio of 21 is used to generate an underexpanded supersonic airflow. Fuel is injected coaxially along the nozzle axis. The tip of the fuel-injection system is tapered to reduce throat blockage of the air nozzle if fuel is injected in transonic airflow. Nevertheless, the partial throat blockage induced by the fuel system increases the effective inlet-to-exit area ratio of the air nozzle, which becomes 25 if fuel is injected right at the throat. Near-field Mach numbers of up to 2.2 (nonswirling) can be obtained under these conditions if the reservoir pressure is increased to the available 9 atm (abs). The air nozzle has swirling capabilities, wherein the axial-tangential-entry technique with four tangential inlets is used to accurately control the degree of swirl imparted to airflow. This technique has been proven in previous research to be an efficient method for generating supersonic swirling jets [17,18]. Thermal flow meters/controllers are used to meter the flow rates of axial and tangential air components with an accuracy of $\pm 1.5\%$ full scale.

The nozzle was machined out of a single aluminum rod. Aluminum was preferred to stainless steel because the former has higher thermal conductivity, which allows for using the nozzle to examine reacting and/or preheated supersonic flows without overheating the nozzle walls. The higher conductivity allows the radiated heat to be dissipated effectively through the thick nozzle walls. The dissipated heat is removed by forced convection of the cold ambient air entrained through the large exterior surface area of the nozzle, which eliminates the need to machine a sophisticated cooling system within the walls. The thickness of nozzle lip was optimized to allow for significant entrainment of ambient air while having adequate rigidity for machining the exit section to the desired surface finish and dimensional tolerance. It should be noted here that although the focus of this study is to examine supersonic mixing under nonreacting conditions, the aluminum nozzle was still used, in order to incorporate wall heat transfer, which was proven to

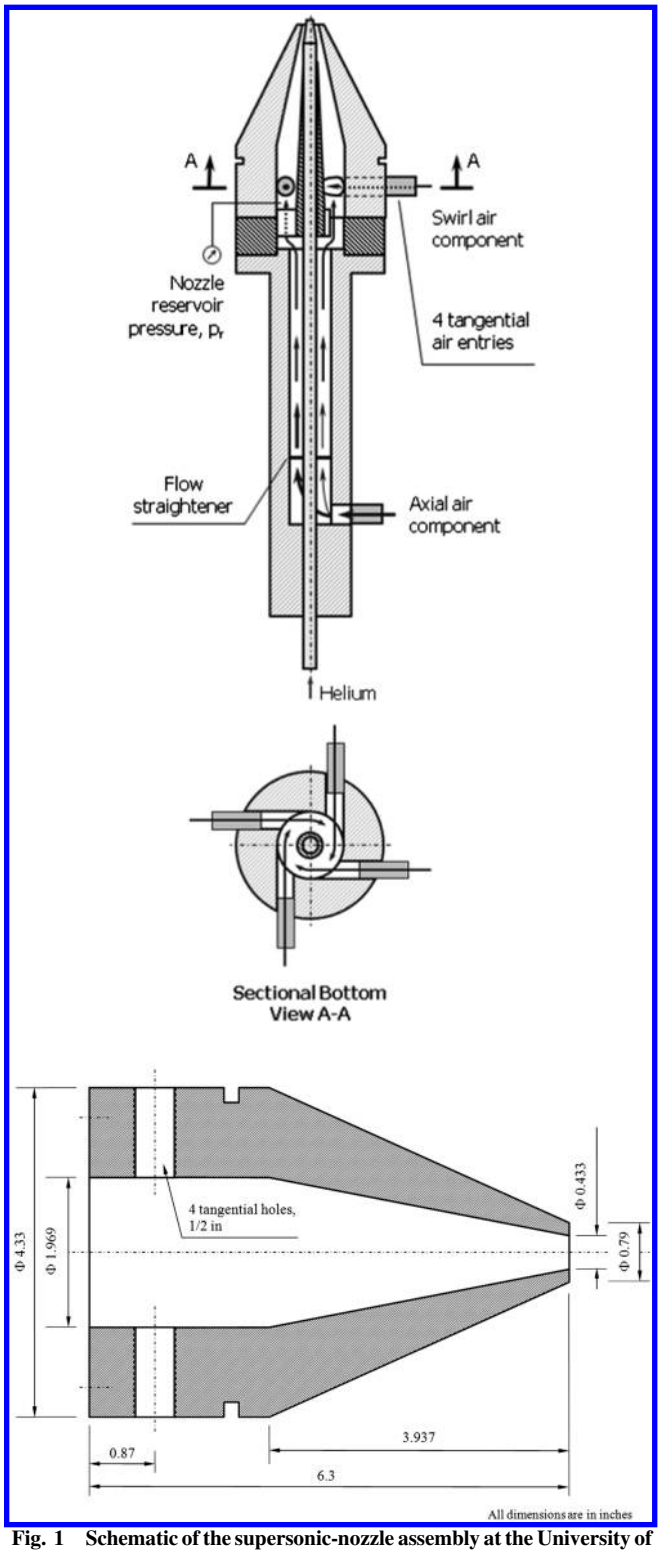

Fig. 1 Schematic of the supersonic-nozzle assembly at the University of Maryland.

significantly affect the evolution of subsonic flow inside the nozzle as well as the properties of the generated supersonic jet [19]. Besides, nonadiabatic nozzle flows with wall heat transfer occur in a number of important practical propulsion applications, including turbofans and turbojet engines, spin-stabilized rockets, and integral rocket/ramjets. Heat transfer is essential for cooling the nozzle walls, especially near the throat section, and it also affects the flow properties significantly.

A support flange upstream of the nozzle ensures and maintains concentricity of the coaxial fuel injection system with respect to air nozzle, especially under swirling conditions. This flange comprises a conical sleeve that embraces the injection system. The sleeve wall thickness decreases in the direction of flow to provide streamlined performance and prevent any blockage close to the nozzle exit. The sleeve is held in place by three spokes extending to the support flange. Their thickness has been optimized to provide rigidity with minimum blockage to the incoming axial component of airflow. It should be noted here that those spokes are located physically upstream of tangential air inlets and do not affect the flowfield of tangential air component. Some wakes are expected to exist in the axial-component flowfield behind the spokes, but the supersonic flow exiting the nozzle was found to be fully axisymmetric, with and without swirl.

A nanosecond condensate-seeded Mie-scattering diagnostic technique was developed and used to nonintrusively highlight the variation of mixedness within the flowfield. The basic principle of this technique is to saturate either the air or fuel flow with the vapor of a volatile material upstream of the nozzle. As the temperature decreases during expansion, some vapor condenses out to form fog or mist of submicron seed particles that are small enough to follow the flow faithfully. When illuminated, these particles emit a Mie-scattering signal that is used to highlight the variation of mixedness.

Diethyl–ether was selected as condensate-seeding material in this study. A schematic of the nanosecond Mie-scattering setup is shown in Fig. 2. Two metered streams of liquid diethyl–ether (one for each air component) are solid atomized, and the resulting spray jets are injected into the lines of high-pressure airflow supplied to the nozzle. The spray droplets evaporate rapidly upon injection, and the vapor mixes thoroughly with air saturating it. Controlled flow rates are injected in order to provide adequate visualization of flowfield while preventing oversaturation of airflow, which can result in the formation of a liquid diethyl–ether film on the internal walls of nozzle or air delivery system.

The supersonic flowfield is illuminated along a centerline plane using a 532 nm Q-switched pulse laser. The nanosecond light duration prevents the seeding particles from creating light streaks on the captured images. The Mie-scattering signal is captured using a digital intensified charge-coupled device (ICCD) camera (Princeton Instruments PI-MAX2:1003 UNIGEN2) operated in synchronization with the laser and aligned at right angles to the laser light sheet. Although the right-angle alignment does not allow for capturing the greater intensity of forward-scattered light, it was used to provide a nonskewed perspective of the illuminated plane. A resolution of 1024×1024 pixels and a gain of 125 were set for all images presented here. This value of gain was found sufficient for boosting the intensity of scattering signal while avoiding undue magnification of the background noise. The intensity distribution on captured images was used to highlight the mixedness distribution, shock structure, shear layers, and slip lines within the flowfield.

III. Numerical Simulation and Assumptions

The commercial CFD-FASTRAN 2008 hybrid large eddy simulation (LES)/RANS code,[‡] provided by ESI Group, was used for all the simulations conducted in this study. Since a free supersonic flow is involved, special emphasis was placed on the choice of boundary conditions that represent the flow surroundings. The entire nozzle assembly was surrounded by a large cylindrical enclosure (Fig. 3) of 40D diameter and 70D length, where D is the nozzle-exit diameter (11 mm), considered to be a good representative of jet size. The 40D enclosure diameter assures that the side boundaries are far enough from the jet in order to maintain constant near-stagnation atmospheric properties at the boundaries. Consequently, the bottom and side enclosure surfaces were assigned the fixed-pressure boundary condition, which matches the constant actual atmospheric ambient pressure. On the other hand, the top side of the enclosure is an extrapolated outlet located 55D away from the nozzle exit (≈78% of the 70D enclosure length). This assures that the flow leaves the

[‡]Data available at http://www.esi-group.com/products/Fluid-Dynamics/cfd-fastran [retrieved 27 September 2010].

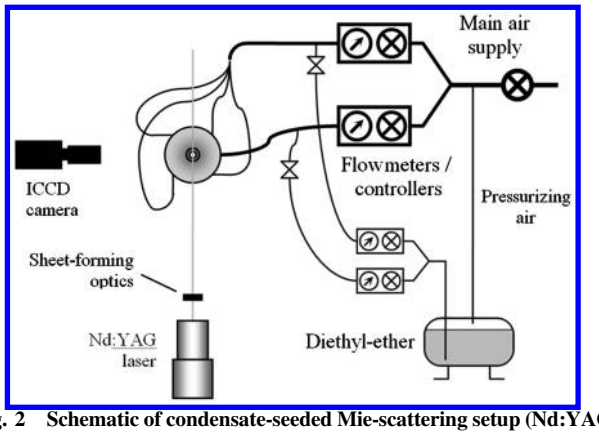

Fig. 2 Schematic of condensate-seeded Mie-scattering setup (Nd:YAG denotes neodymium-doped yttrium aluminum garnet).

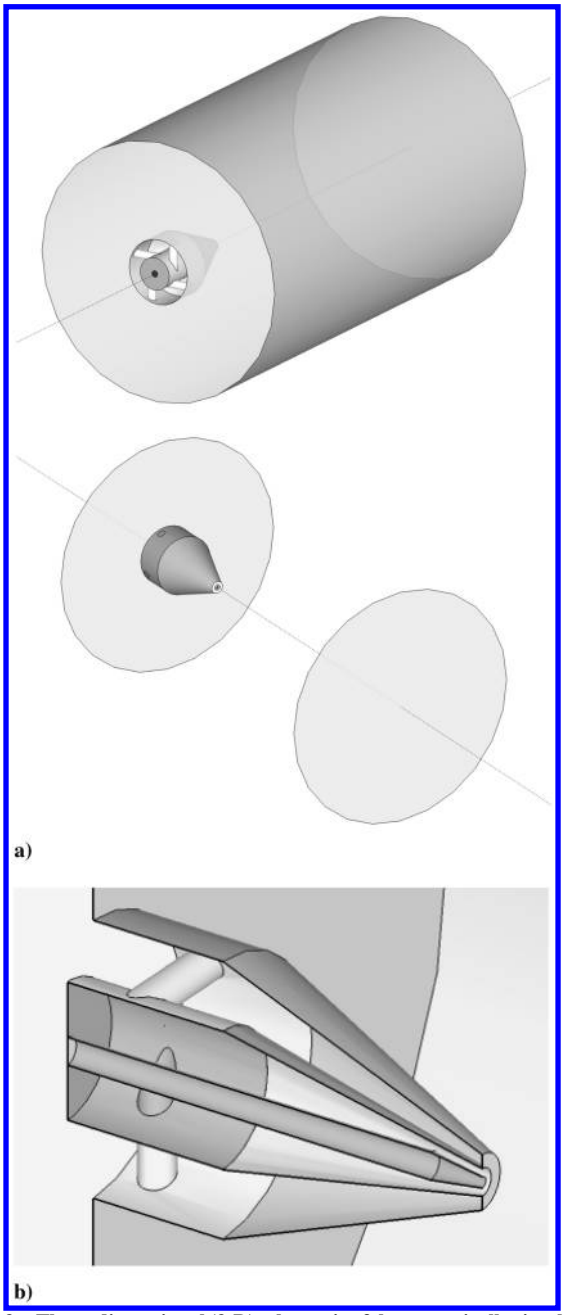

Fig. 3 Three-dimensional (3-D) schematic of the numerically simulated geometry: a) large cylindrical enclosure and b) zoom-in cutaway highlighting the nozzle details.

simulated geometry shock wave free, since it was observed experimentally that complete transition to subsonic speeds occurs at about 30D downstream of the nozzle exit.

Axisymmetry was enforced; that is, only one quadrant of the geometry depicted in Fig. 3 was simulated. Special emphasis was placed on the level of cell skewness. The simulated geometry was subdivided into individual volumes, each meshed separately, in order to keep the skewness level of the most skewed cell below 0.5 (see Fig. 4a). A variable-size grid was generated with tetrahedral cells and a grid spacing ranging from 0.01 to 2.0 mm (see Fig. 4b). Grid spacing is defined here as the longest edge of the cell. Tighter meshing was implemented near and at the critical geometry locations: e.g., the exits of the nozzle and fuel-injection system. Mesh dependence was carefully examined through the examination of multiple levels of mesh tightness (see Fig. 4c). A total of 7,166,860 nodes per quadrant yielded the desired accuracy. Higher tightness levels did not result in significant accuracy enhancement; thus, they were thus not considered in order to optimize the computational time.

Four subgrid RANS turbulence models from the FASTRAN library were tested for their capabilities to accurately predict a free swirling supersonic jet, namely, the k-ε (renormalization group based [20]), k-ω, Spalart–Almaras, and Baldwin–Lomax [21] models. The most suitable one was chosen after comparing the computational variations of centerline total and static temperatures and Mach number in the swirling supersonic flowfield of case 0s to corresponding experimental data. Figure 5a shows the polyoxymethylene (Delrin) probes used for temperature measurement. The probes were designed to have the necessary structural rigidity while being streamlined to induce the least disturbance to a swirling supersonic flow. Type-K thermocouples were used in both temperature probes with junction diameters of 0.2 mm (∼0.02D). The tip of the total-temperature probe has a diameter of 1 mm (∼0.1D), which is five times the junction diameter, in order to ensure effective flow

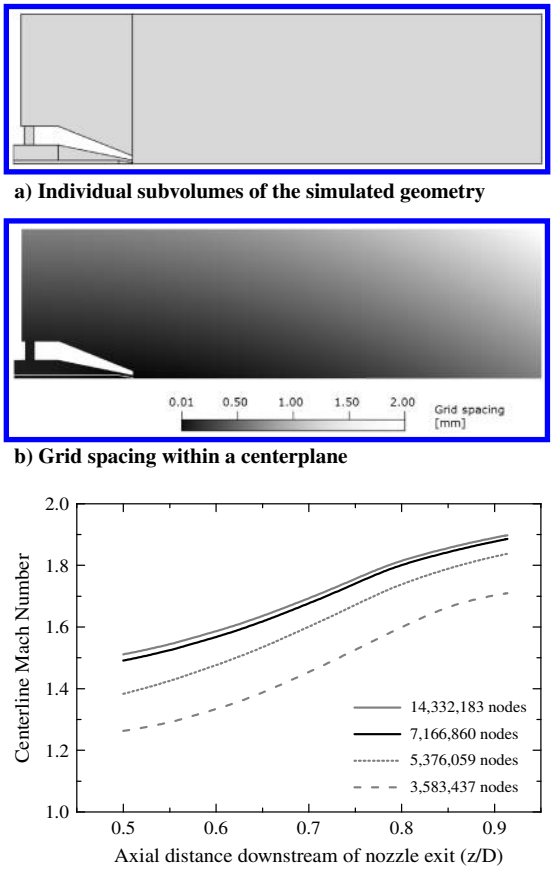

a) Individual subvolumes of the simulated geometry

b) Grid spacing within a centerplane

c) Mesh dependence (case 0s)

Fig. 4 Details of the numerical grid: a) individual subvolumes, b) grid spacing within a centerplane, and c) mesh dependence (case 0s).

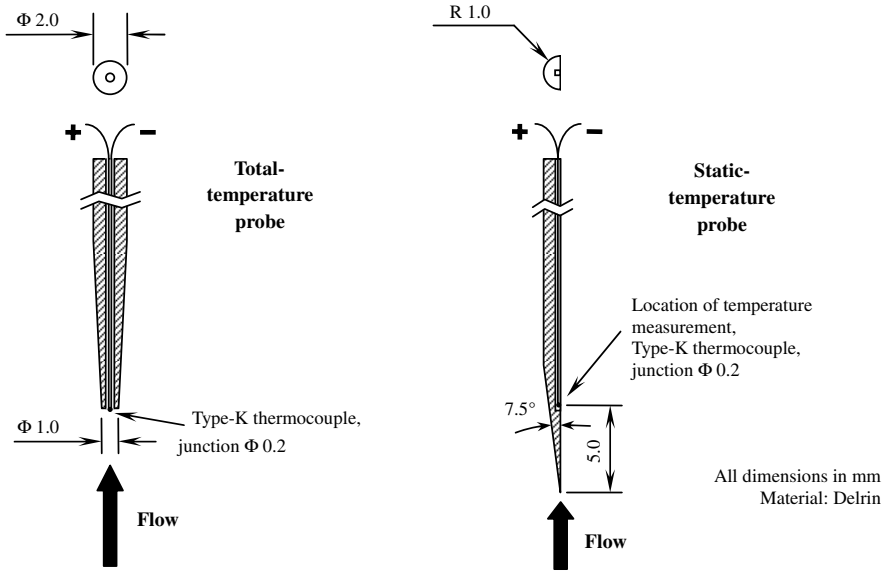

a) Schematic presentation of the probes used for code validation

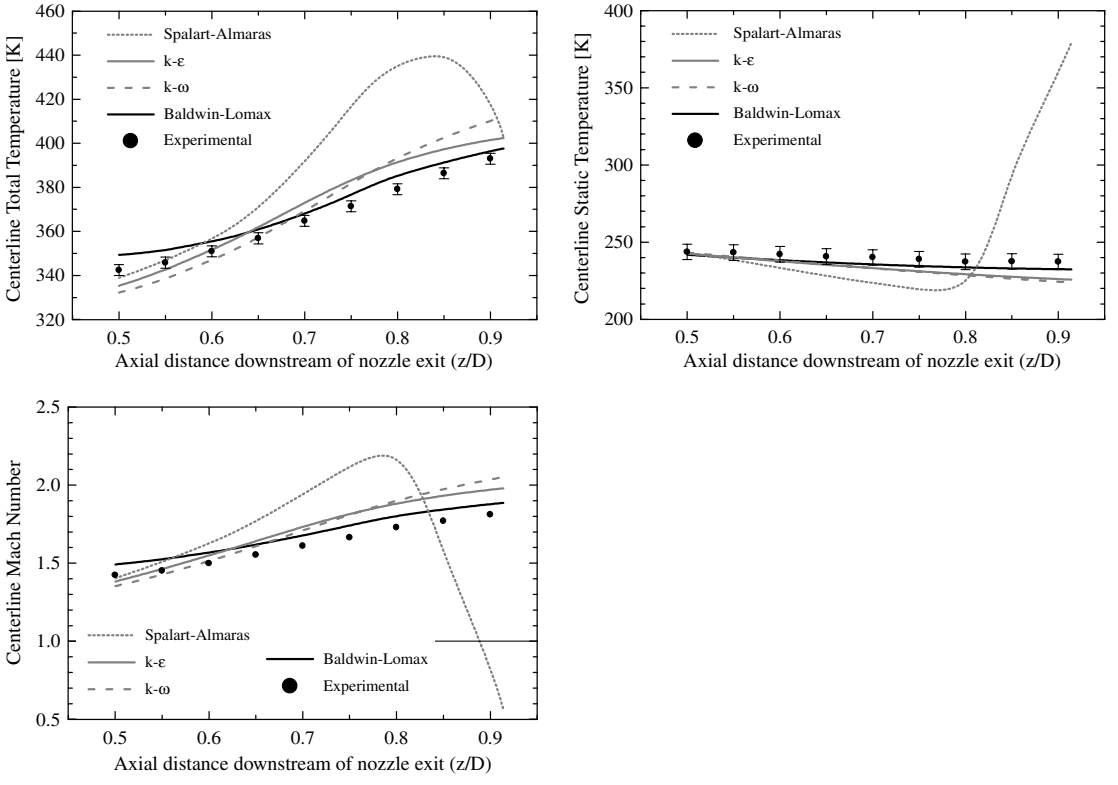

b) Choice of RANS turbulence model (case 0s)

Fig. 5 Validation of the numerical code: a) schematic presentation of the probes used for code validation and b) choice of RANS turbulence model (case 0s).

deceleration to stagnation while minimizing the stresses on the delicate thermocouple wiring. The measured total temperature was associated to the axial position of the nose of the bow shock that precedes the probe. The static-temperature thermocouple was glued into the probe centerline groove while making sure that the junction remains bare and does not protrude outside the groove. The distance between the junction and the probe tip could not be reduced below 5 mm because of the 7.5° half-cone angle of the probe tip and structural-rigidity constraints. Assuming zero radial and tangential-velocity components at the centerline (which agrees with the findings of Naughton et al. [11]), the Mach number was calculated using the adiabatic stagnation equation $T_0 = T[1 + 0.5(\gamma - 1)M^2]$ with a constant value of 1.4 for the ratio of specific heats.

The measured centerline total and static temperatures within the axial range $0.5 < z/D < 0.9$ of case 0s are plotted in Fig. 5b along with the resulting calculated Mach number. Although the latter was not directly measured, its data points were denoted experimental because they result from measured values of total and static temperature. Also plotted in Fig. 5b are the variations of all three parameters within the same axial range from four different numerical simulations of case 0s, each examining one of the aforementioned potential turbulence models. It can be clearly seen that the Baldwin–Lomax model provides the best representation of the experimental data among the four examined models. This conclusion is unanimous, based on all three parameters. The temperatures are estimated with 98% accuracy, while the error in Mach number is

within 5%. Although several modifications of the Baldwin–Lomax model have been published in the literature, in an attempt to enhance its prediction capabilities, it should be noted here that FASTRAN is not an open-source code, and none of those modifications are available in the code. Nevertheless, the obtained degree of accuracy with the basic Baldwin–Lomax model was considered acceptable for the scope of this study.

In light of the aforementioned code-validation comparison, it can be concluded that the Baldwin–Lomax turbulence model is capable of predicting free supersonic swirling flows with good accuracy. This negates the common generic belief that this model poorly predicts swirling flows, which might be true under subsonic conditions but not under supersonic ones, based on the findings of this study. Had the modified versions of the Baldwin–Lomax model been available in the FASTRAN code library, better prediction accuracy might have been achieved. The reader is referred to previous studies conducted by the authors [22] and Abdelhafez et al. [23], where the Baldwin–Lomax model was successfully implemented in simulating confined supersonic flows using the hybrid LES/RANS FASTRAN code.

Calculation of the viscosity and conductivity was based on the kinetic theory of gases. A turbulent Schmidt number of 0.9 was used, and the mass diffusivity was calculated based on Fick's law with a Schmidt number of 0.5. A turbulent Prandtl number of 0.9 was used to calculate the turbulent conductivity. Similar to the experimental conditions, the total temperature at the air inlets was kept fixed at 300 K, while the total pressure was maintained at 7.91 bar for the nonswirling cases and 8.82 bar for the swirling ones. The 8.82 bar value was carefully chosen to ensure a common air flow rate of 175 g/s. The need for higher nozzle reservoir pressure with swirl is explained in detail in a pertinent previous study by the authors [19]. The total pressure and temperature at the air inlets were preserved throughout the iteration process in each examined case until convergence was attained. Owing to the relatively large cross-sectional areas of the air inlets, the entrance velocity of air was only 9.7 m/s, resulting in almost identical inlet stagnation and static conditions.

The nozzle walls were set to be isothermal at 280 K, based on multiple temperature measurements of the nozzle interior and exterior walls. This is attributed to the aforementioned fact that the nozzle is made of aluminum, which has a high thermal conductivity, thus allowing the nozzle to act as a near-isothermal body. On the other hand, the walls of fuel-injection system were set to be adiabatic, because the injection system is immersed almost totally into the nozzle and conditioning chamber, which allows for negligible amounts of heat to be conducted axially upstream through the thin walls of fuel system. Moreover, it is made of stainless steel that has a much lower thermal conductivity (relative to aluminum).

The initial simulation conditions were set for all cases at 1 atm static pressure, 300 K static temperature, 9.7 m/s axial velocity, and zero radial and tangential velocities. Consequently, the simulation incorporated the transient behavior as the high-pressure air expands and marches from the geometry inlet to the exit. An initial Courant–Friedrichs–Lewy number [24] of 0.1 was chosen that increased to unity as convergence was approached. Time integration is implicit, where a point Jacobi scheme was used, and a backward Euler discretization was implemented. Each case included 20,000 iterations. Convergence to 10^{-6} residuals was usually attained after 18,500–19,500 iterations.

IV. Test Matrix

The effect of swirl is investigated here by forwarding the entire airflow to the tangential entries of the nozzle. This allows for examining a single degree of swirl, namely, the maximum attainable one. Following a definition used for incompressible swirling jets [17,25], a nozzle-based geometrical swirl number, S_g, for air is defined as

$$S_g = \left(\frac{\pi r_o R_o}{A_t}\right)\frac{m_t}{m_a + m_t} \tag{1}$$

where $(\pi r_o R_o/A_t) = 0.68$ for the geometry of the nozzle and its tangential entries, and m_a and m_t are the axial and tangential components of airflow, respectively. The parameters r_0, R_0, and A_t are basically defined for a rectangular tangential inlet. However, since the tangential inlets are circular in this study, effective values had to be calculated for those parameters. The calculations have been omitted to avoid diverting the reader's attention from the main flow of context. The reader is, however, encouraged to consult [17] for the details.

All swirling cases in this study have the same nozzle-based geometrical swirl number of 0.68. The term nozzle-based refers to nozzle operation in the absence of coaxial injection system, since the presence of axial injection reduces the geometrical swirl number down to only 0.36 [26]. This significant reduction rendered the examination of the effect of swirl feasible only at its maximum attainable degree.

In addition to an extensive examination of the effect of swirl on shock structure and mixing, the effects of two flow parameters are investigated here under both nonswirling and swirling conditions, namely, the relative Mach number (M_{rel}) and air–fuel DR. The relative Mach number is defined here as

$$M_{\text{rel}} = \frac{v_{\text{air}} - v_{\text{fuel}}}{0.5(a_{\text{air}} + a_{\text{fuel}})} \tag{2}$$

This definition relates the difference in freestream velocities between fuel and air to the average speed of sound. It should be noted that the fuel simulant is injected here at velocities smaller than those of transonic airflow in most of the examined cases. Therefore, v_{fuel} is subtracted from v_{air} in the previous definition in order for M_{rel} to have positive values. Nevertheless, in a few extreme cases, the fuel simulant is injected at velocities greater than those of airflow, and the corresponding values of M_{rel} are indicated here without neglecting their negative signs in order to highlight the unique nature of those cases; that is, $v_{\text{fuel}} > v_{\text{air}}$.

Each examined case in this study has a nominal value of M_{rel} that describes the injection conditions within that case. Since fuel is injected at the throat of air nozzle in all cases to be presented here, the nominal value of M_{rel} was calculated for each case using the fuel-injection velocity and the sonic (throat) value of v_{air}. A comparison based on nominal M_{rel} thus allows for examining the effect of fuel-injection conditions on the global features of flowfield, including shock structure and mixing. Under nonswirling conditions, sonic v_{air} was found to be 323 m/s, based on isentropic ideal-gas relations. No similar simple calculations of v_{air} could be carried out for the swirling cases. Nevertheless, the results of numerical simulations revealed that the magnitude of sonic v_{air} is 329 m/s with swirl, which is almost equal to the nonswirling value. This fact allowed for examining the same nominal values of M_{rel} under both nonswirling and swirling conditions carried out in this study.

The shock structure and all properties of airflow, including the aforementioned values of v_{air}, depend on air total pressure and temperature. Both were kept constant at 7.91 bar and 300 K, respectively, for all nonswirling cases presented in this study, which resulted in a fixed air flow rate of 175 g/s. It was noticed, however, that imparting swirl to airflow at the same nozzle reservoir pressure of 7.91 bar results in reduced mass flow rate through the nozzle. This observation agrees with the findings of many previous studies (see [19] for an extensive review). It was shown that imparting swirl to the airflow results in additional choking of the nozzle: i.e., a lower mass flow rate compared with the corresponding nonswirling conditions at the same reservoir pressure. A theoretical limit of no flow was even predicted at an infinitely large swirl number. Therefore, a higher reservoir pressure is necessary to maintain the same flow rate through the nozzle. It was found in this study that a value of 8.82 bar yields identical air flow rates of 175 g/s in the nonswirling and swirling cases.

Table 1 lists the test matrix for the results presented here. A total of 48 cases have been examined (24 nonswirling cases plus their swirling counterparts). Case pair 0 uses no fuel injection and serves to quantify the effect of swirl on supersonic flowfield and shock strength. Case pairs 1–13 examine the effect of M_{rel}, wherein the injectant is helium. The injection velocity of helium is changed to

Table 1 Test matrix[a]

Case	Injected Gas	M_{rel}	DR	Experimental	Numerical
0 and 0s	Air only; no fuel injection				
		Effect of M_{rel}			
1 and 1s	Helium	0.44	35.50	✓	✓
2 and 2s		0.41		✓	
3 and 3s		0.39		✓	
4 and 4s		0.37		✓	
5 and 5s		0.35		✓	✓
6 and 6s		0.32		✓	
7 and 7s		0.30		✓	
8 and 8s		0.28		✓	
9 and 9s		0.26		✓	✓
10 and 10s		0.21			✓
11 and 11s		0.00			✓
12 and 12s		−0.21			✓
13 and 13s		−0.48			✓
		Effect of DR			
14 and 14s	100% helium	0.21	35.50		✓
15 and 15s	80% helium/ 20% argon		12.68	✓	✓
16 and 16s	70% helium/ 30% argon		9.60	✓	
17 and 17s	60% helium/ 40% argon		7.72	✓	
18 and 18s	50% helium/ 50% argon		6.46	✓	✓
19 and 19s	40% helium/ 60% argon		5.55	✓	
20 and 20s	30% helium/ 70% argon		4.86	✓	
21 and 21s	20% helium/ 80% argon		4.33	✓	✓
22 and 22s	50% helium/ 50% krypton		3.24		✓
23 and 23s	50% argon/ 50% krypton		2.29		✓

[a] Constant parameters: air total temperature at inlet = 300 K; nozzle reservoir pressure = 7.91 bar (nonswirling), 8.82 bar (swirling); and geometrical swirl number for swirling cases, $S_g = 0.36$

induce different values of nominal M_{rel}. The effect of DR is studied through case pairs 14–23, wherein the injectant comprises different inert-gas mixtures. The mixture composition is varied to change mixture density and, consequently, DR. To maintain constant M_{rel} throughout the analysis for DR, the injection velocity was adjusted to account for the changes in a_{fuel} due to the varying injectant composition. The examined values of M_{rel} and DR were carefully selected according to the following criteria:

1) The experimentally attainable ranges are spanned with narrow intervals in order to quantify the examined effects accurately. For example, M_{rel} is examined over the range 0.44–0.26 at eight intervals, while DR is covered in the range 12.68–4.33 at six intervals.

2) The numerical simulations span the experimental ranges with wide intervals: i.e., one simulation at the beginning of the range, one at midrange, and one at the end. Thus, case pairs 1, 5, and 9 of the M_{rel} analysis were examined both experimentally and numerically. The same applies for case pairs 15, 18, and 21 of the DR analysis.

3) The numerical simulations extend beyond the experimental ranges to broaden the scope of analysis and qualitatively examine how accurate the experimental trends would be extrapolated beyond the originally examined ranges.

Note that case pairs 10 and 14 (Table 1) are identical, as they have the same fuel simulant (helium), M_{rel}, and DR. These two case pairs link the analyses of M_{rel} and DR. Also note that the letter s next to a case number denotes a swirling case.

V. Results and Discussion

A. Shock Structure (Nonswirling)

Although the focus of this study is mixing, knowledge of the complicated shock structure of the examined flowfield is of critical importance to understand the findings presented here. This subsection is thus devoted to briefly explain the shock structure, both without and with fuel injection. For a comprehensive analysis of this shock structure, the reader is referred to [12].

The shock structure of simple underexpanded supersonic flow is shown schematically in Fig. 6. As can be seen, the structure comprises a shock-cell unit that gets repeated periodically to form a shock-cell train. This unit can be described as follows. Axial underexpanded flow undergoes an expansion fan and turns outward. The freejet boundary adapts accordingly and turns outward as well. Passing again through the expansion fan, the outward flow turns back to axial. As the expansion fan meets the boundary, it reflects into a compression fan that coalesces later into the intercepting shock wave. The annular flow adjacent to the boundary turns inward through the compression fan, and the boundary again adapts by turning inward as well. For slightly underexpanded nozzles, this intercepting shock reflects directly into a reflected shock at the centerline, forming the familiar diamond configuration. However, as the pressure ratio across the nozzle is increased, this reflection no longer takes place at the centerline, and a Mach disk is formed. The reflected shock turns the inward annular flow back to the axial direction. Since the Mach disk maintains the axial direction of core flow, the entire flow is now axial again. As the reflected shock impinges on the free-flow boundary, it reflects into an expansion fan, starting another shock-cell unit. The repetition of units is continued until viscous effects become predominant, and this structure is no longer observed.

In the presence of a coaxial injection system, the shock structure differs significantly from the simple one described previously. Figure 7 [12] shows a schlieren image as well as a schematic of the shock structure of free nozzle flow in the presence of the coaxial injection system but with no fuel injection. Two distinct substructures are identifiable from the schlieren image and highlighted in the schematic. The first substructure is the simple nozzle-rim structure discussed previously. A new substructure, namely, a separated base flow, is generated due to the existence of coaxial injection system. It

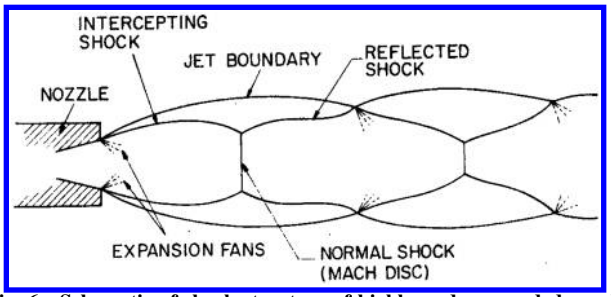

Fig. 6 Schematic of shock structure of highly underexpanded nozzle flow.

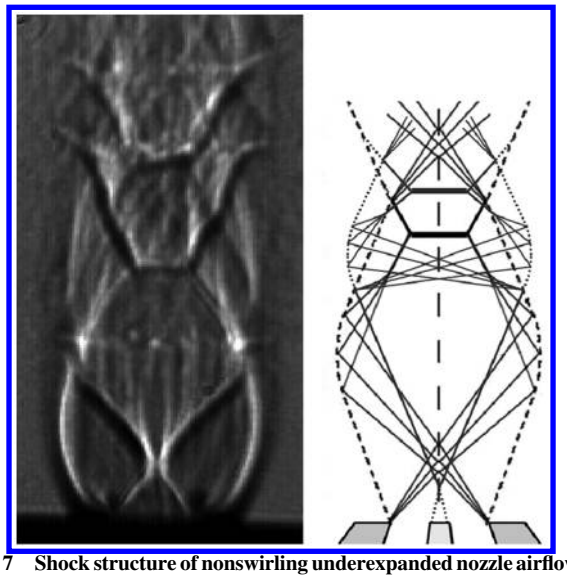

Fig. 7 Shock structure of nonswirling underexpanded nozzle airflow in presence of coaxial injection system with no fuel injection [12].

should be noted that both substructures are not fully independent of each other. The presence of each affects the other. This interaction is, however, not indicated on the schematic in Fig. 7 for easier understanding of the newly introduced separated base flow. Indicated here is how each structure would propagate if fully independent of the other. From this point forward, the nozzle-rim and injection-system substructures will be denoted as primary and secondary shock structures, respectively, in this study.

The secondary structure starts with a separated base flow, where the airflow generates an inner conical boundary that completes the cone-frustum shape of fuel system tip. At the centerline, the flow collapses into itself, generating a conical shock wave that turns the flow back to parallel. This shock wave impinges on the outer flow boundaries just downstream of the impingement location of the nozzle-rim expansion fan. The outer boundaries are altered by the impingement of that conical shock, as observed from Fig. 7. The shock reflects into an expansion fan that creates its own compression fan, intercepting shock, Mach disk, and reflected shock, similar to the primary structure. Both Mach disks of primary and secondary structures appear distinctly in Fig. 7.

The effect of coaxial fuel injection is shown in Fig. 8 [12]. Helium is used as fuel simulant. As observed, the secondary shock structure is altered slightly. A shear layer develops in place of the former inner conical boundaries of airflow. Because of the presence of helium, the shear layer does not converge to a sharp point at the centerline. Moreover, due to the curved shape of this shear layer, the airflow undergoes gradual compression through a compression fan, which collapses later into a shock wave that generates the secondary shock substructure.

B. Supersonic Flowfield

Figure 9 shows the Mie-scattering images of cases 0 and 0s from Table 1. The horizontal white lines highlight the first primary Mach disks in cases 0 and 0s. Several important observations can be made from Fig. 9. First, the dark core region downstream of nozzle exit has almost no diethyl–ether seeding particles, hence its dark appearance. It is believed to be composed of toroidal vortices of subsonic flow, where kinetic energy is dissipated in viscous heating. Moreover, the static pressure and temperature within this region are equal to the corresponding stagnation values of the surrounding supersonic flow. Diethyl–ether particles are thus heated up and reevaporated, which explains the dark appearance of the core region. It can be noted here that swirl strongly affects the size of this region. It is forced by the greater nozzle-rim expansion fan of swirling flowfield to take a smaller size with curved boundaries, which explains the schematic to the right in Fig. 9.

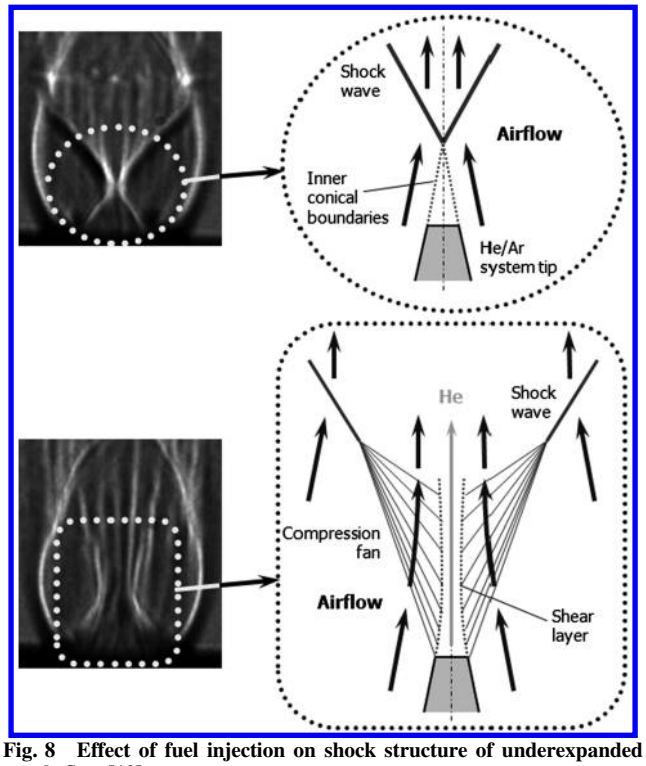

Fig. 8 Effect of fuel injection on shock structure of underexpanded nozzle flow [12].

The conical shock wave of the secondary shock structure is also identifiable in the Mie-scattering images, and so are all the other major shocks of flowfield, such as intercepting shock, Mach disk, and reflected shock. The second important observation to be made here is that the intensity of Mie-scattered light increases after the flow passes through each shock. This is attributed to flow compression. The dense fog of seeding particles downstream of a shock wave scatters more light. Based on this observation, it can be concluded which shocks are stronger than others. The intercepting shock, for example, is distinctly stronger than the reflected one. The Mach disk is an

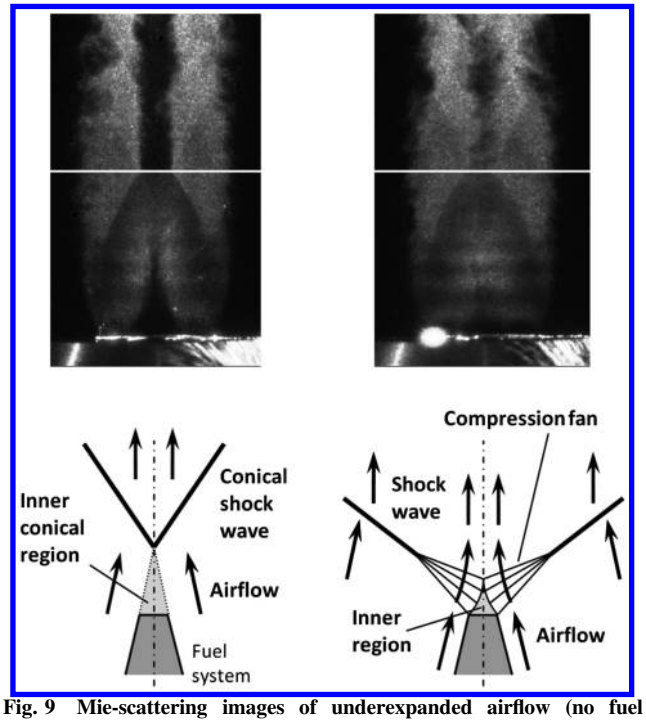

Fig. 9 Mie-scattering images of underexpanded airflow (no fuel injection): case 0 (nonswirling, reservoir pressure = 7.91 bar) (left) and case 0s (swirling, reservoir pressure = 8.82 bar) (right).

exception of this rule. Being a normal shock, it decelerates the incoming core flow to subsonic speeds, thus raising its temperature significantly. The higher temperature is believed to cause reevaporation of the liquid diethyl–ether seeding particles. Their absence explains the dark appearance of subsonic core flow downstream of the Mach disk. This subsonic core is separated by slip lines from supersonic annular flow. The considerably lower temperature of this annular flow preserves the existence of liquid seeding particles.

The most remarkable observation to be made from the Mie-scattering images in Fig. 9 is that a moderate degree of swirl results in noticeable mixing enhancement. Although cases 0 and 0s use no fuel injection, enhanced mixing with swirl is still obvious between different regions of the air flowfield. A clear proof is evident in the smeared slip lines and narrower subsonic core downstream of first primary Mach disk in the swirling flowfield. Enhanced mixing occurs between the supersonic and subsonic sides of slip lines, which is absent across the sharp slip lines of the nonswirling flowfield. Note that the presence of visible seeding particles inside the warmer subsonic core means that 1) the annular supersonic flow is the source of these particles, and 2) swirl enhances the mixing of the core and annular flows across the slip lines, thus lowering the temperature of core flow down to the level where it can sustain the presence of liquid seeding particles. To help understand the positive effect of swirl on mixing, consider Fig. 10 [12], where the orientation of the axial and tangential-velocity components (v_a and v_t) with respect to the flow shock structure is depicted. It can be seen that v_a is normal to the Mach disk and gets decelerated to a subsonic value within the core flow. However, v_a is oblique to the reflected and intercepting shocks and thus remains supersonic in the annular flow. On the other hand, v_t is parallel to the entire shock structure and thus undergoes no changes across any of its features. Since the small geometrical swirl number ($S_g = 0.36$) of case 0s results in a small subsonic v_t [19], the velocity magnitude is subsonic within the core flow but supersonic within the annular one. Neglecting any changes in v_t across the thin slip lines downstream of the Mach disk, the significant difference in v_a results in different directions of the subsonic and supersonic velocity vectors (see Fig. 10). This change in direction does not exist in the nonswirling flowfield, as both velocity vectors are intrinsically parallel in the absence of a tangential component. Since the slip lines can be basically treated as a shear layer, the enhanced mixing observed in case 0s can be attributed to the swirl-induced change in direction of velocity vector across the slip lines.

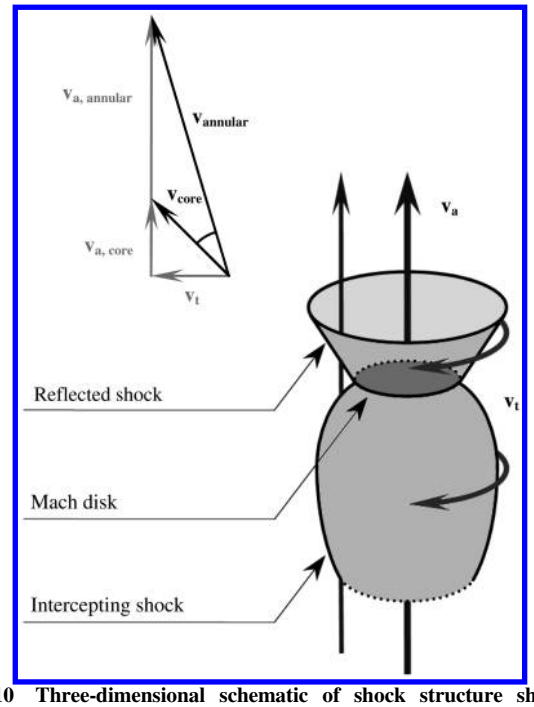

Fig. 10 Three-dimensional schematic of shock structure showing orientation of axial and tangential-velocity components with respect to Mach disk and intercepting and reflected shocks [12].

It should be noted at this point that the Mie-scattering images can only be analyzed qualitatively; that is, the intensity scale of scattered light cannot be converted accurately to a quantitative mixture-fraction scale, even when fuel is injected into the airflow. This is attributed to the nature of condensate seeding, where the local temperature and pressure strongly affect the size, concentration, and even the presence of seeding particles. The obtained light-intensity scale is thus a complicated function of pressure, temperature, and mixture fraction. Decoupling the three individual effects is an intricate process. For this reason, the aforementioned validation of numerical code was based on temperature and not mixture fraction.

C. Effect of Relative Mach Number M_{rel}

Having attained good understanding of the effect of swirl on supersonic flowfield, the analysis proceeds to examine the effect of fuel injection at different relative Mach numbers. Please note that swirl is imparted to air at matched mass flow from this point forward; that is, all swirling cases have the same mass flow rate for the nonswirling ones (175 g/s). This implies that the swirling cases have the elevated nozzle reservoir pressure of 8.82 bar. Matching of air mass flow allows for a fair comparison between the different case pairs, primarily from the point of view of mixture fractions and mixedness.

The effect of M_{rel} is examined in case pairs 1–13, given in Table 1. Case pair 11 represents a unique condition, where fuel is injected at the throat velocity of air, resulting in M_{rel} of zero. Case pairs 12 and 13 represent the extreme situations, where fuel is injected at velocities higher than the throat velocity of air. The corresponding values of M_{rel} are indicated here without neglecting their negative signs in order to highlight the unique nature of those two case pairs.

Keeping all airflow properties constant, the flow rate of fuel (simulated by helium) was changed to induce different fuel velocities and thus multiple values of M_{rel}. The injection Mach number of helium was kept below 0.3 (except in case pairs 12 and 13) in order to maintain a constant helium density and to avoid compressibility effects on the helium side of air/helium shear layer. The resulting DR was about 35.5 for most cases. The supply pressure of helium was carefully selected for each case pair to match the total pressures of helium and air at injection.

Figure 11 shows the effect of M_{rel} at constant DR. The experimental results (Mie-scattering images) are depicted in Fig. 11a, while the numerical results in the form of fuel mixture fraction profiles are shown in Fig. 11b. The nonswirling cases are depicted in the top row, while the bottom row contains the swirling cases. The values of M_{rel} and injection Mach number of each case pair are indicated at the top of each column.

The most remarkable observation to be made from Fig. 11 is that the air–fuel shear layer initiates with a negative angle that transforms later to positive. In other words, the cross-sectional area of core flow converges initially to a minimum value before propagating divergently as expected. Figure 12 helps explain this observation. Shown are the axial variations of computed centerline Mach number and fuel mass fraction for different values of M_{rel} under nonswirling and swirling conditions. Note that subsonic injection is implemented throughout the analysis of M_{rel}. However, the centerline Mach numbers are observed to increase from the subsonic injection values to supersonic maxima of 1.7–2.1. The only possible way for the subsonic core flow to expand to supersonic speeds is to resemble a convergent–divergent nozzle. This can only be achieved if the cross-sectional area of core flow initially converges to a throat before diverging again. The creation of a throat allows the core flow to transition from subsonic to supersonic speeds. To attain further understanding of the location of core-flow throat within flowfield, Fig. 13 shows how the axial position of this throat varies with M_{rel}. Notice that at high M_{rel} (i.e., low injection velocities), the core flow propagates axially for about $0.5D$ with a negative-shear angle.[§] The

[§]The angle between the shear layer and the streamwise direction is termed shear angle. It is considered positive if the jet diameter increases (i.e., expanding jets) and negative if the diameter decreases.

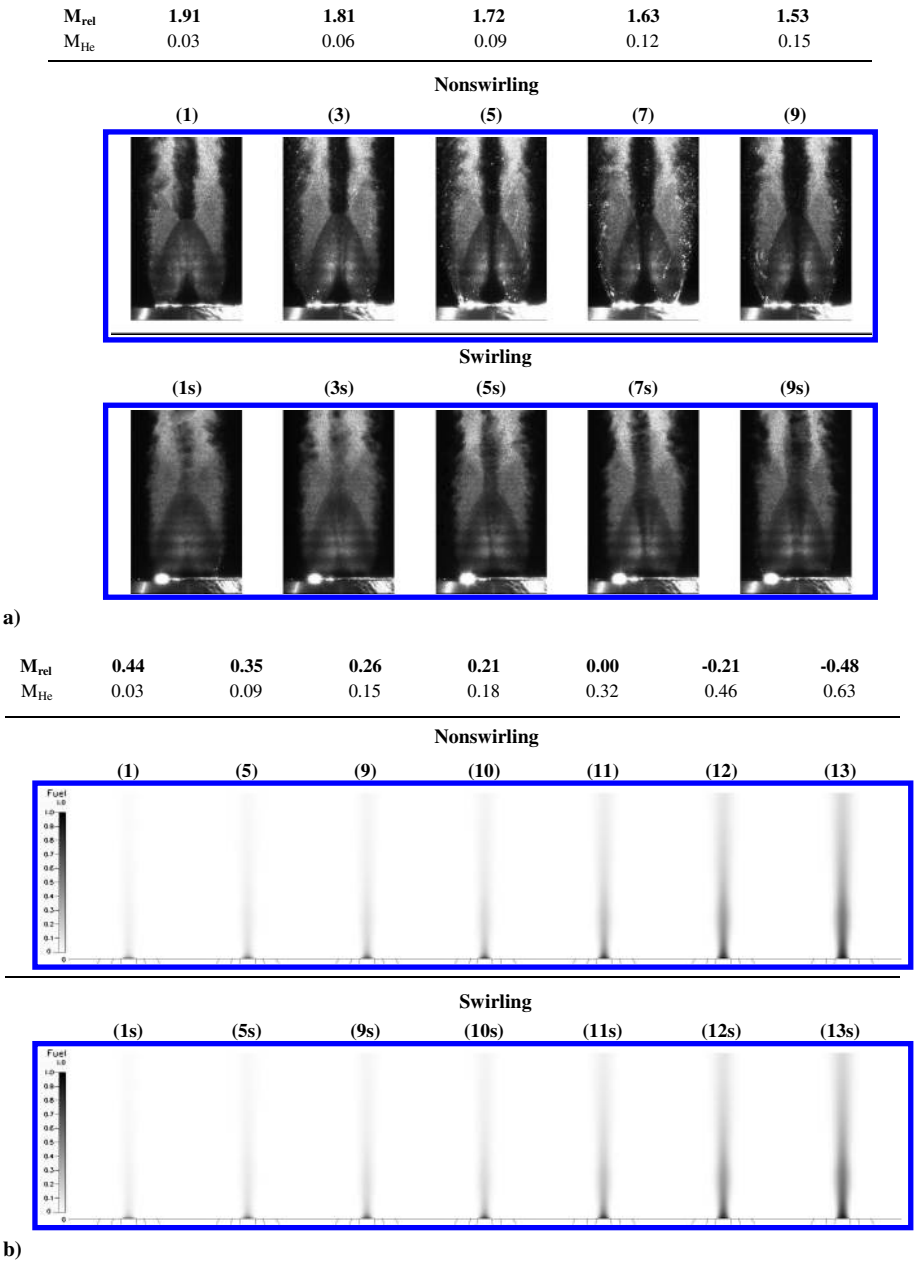

Fig. 11 Effects of M_{rel} at constant DR of 35.50: a) Mie-scattering images and b) numerical results (fuel mass fraction profiles).

throat of core flow, however, approaches nozzle exit at low M_{rel} (high injection velocities), and negative-shear-angle propagation is only confined to an axial distance of $0.25D$.

Another important observation to be made from Fig. 12 is that the initial mixing rate up to z/D of about 0.2 is observed to be affected significantly by the compressibility of fuel injection. Note that incompressible injection is implemented up to M_{rel} of 0.21, whereas case pairs 11–13 (0.00 to −0.48) use compressible injection. Higher M_{rel} demonstrate superior mixing. The mixture fraction of fuel drops to centerline values as low as 0.13, which demonstrates how short the potential core of fuel is at high M_{rel}.

Combining the analyses of core-flow throat and initial mixing rate, it can be concluded that fuel injected at low subsonic Mach numbers (high M_{rel}) has to propagate for longer axial distances with a negative-shear angle before the fuel-rich core flow reaches a throat, after which it propagates supersonically. This is advantageous from two aspects. First, increasing the distance between core throat and injection point allows for more mixing to take place across a supersonic/subsonic shear layer, which is significantly more effective than the fully supersonic one downstream of core throat. This is evident in the rates of decay in centerline fuel mass fraction in Fig. 12. Notice that the decay rates are significantly higher upstream of the core throat, which indicates better mixing quality. The second advantage of low injection Mach numbers is that a negative-angled shear layer propagates with a radially inward component, which allows it to confine the fuel-rich core flow more effectively. This core is thus consumed more rapidly by the growing shear layer, which results in superior mixing at high M_{rel}. The Mie-scattering images in Fig. 11 confirm this discussion. It can be clearly observed that the high M_{rel} of case pair 1 results in near-complete mixing of the helium jet with surrounding airflow. Mixing deteriorates gradually as M_{rel} is decreased, which is evidenced in the increasing darkness and size of the unseeded helium-rich core flow.

The analysis of M_{rel} is concluded here by highlighting the effect of swirl. The first outcome of applying swirl is significant mixing enhancement. This has been expected and can be clearly observed from the Mie-scattering images in Fig. 11. Notice that the unseeded core flow in all swirling cases has considerably brighter shades and smaller sizes. Enhanced mixing with the surrounding supersonic airflow explains the presence of seeding particles inside the core flow in swirling cases, whereas the helium-rich core flow in nonswirling cases are particle free.

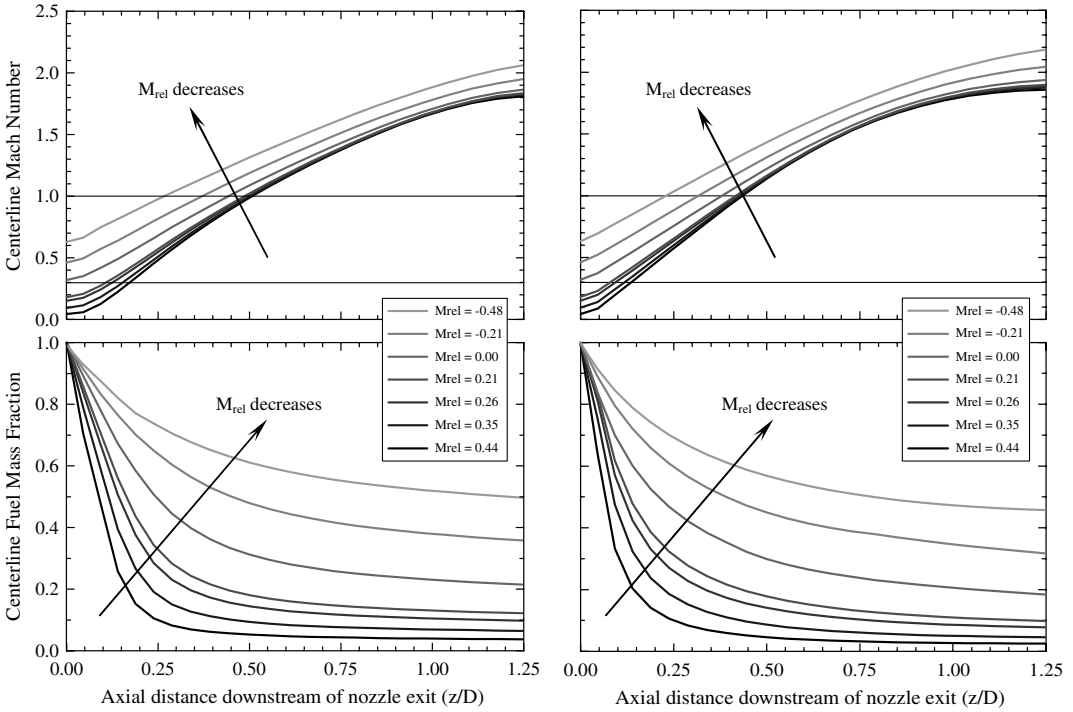

Fig. 12 Axial variations of centerline Mach number and fuel mass fraction for different values of M_{rel} under nonswirling (left) and swirling (right) conditions.

Figure 12 confirms the positive effect of swirl on mixing. It can be seen that swirl induces an overall reduction in centerline fuel mass fraction, regardless of M_{rel}, which suggests better mixing. The effect of swirl is significant at low z/D (as observed from the higher decay rates of fuel mass fraction) and fades gradually as the flow progresses further downstream. Figure 14 sheds more light on this observation by comparing the percentage swirl-induced mixing enhancement at z/D of 0.1 and 1.25 over the examined range of M_{rel}. This percentage is defined as

$$\left(\frac{x_{\text{nonswirling}} - x_{\text{swirling}}}{x_{\text{nonswirling}}}\right)_{\text{centerline}} \tag{3}$$

At high M_{rel}, mixing is enhanced by about 30% after $0.1D$ of flow travel, and an additional 5% over only the axial spans of $0.1D$ to $1.25D$. This agrees with the findings of Abdelhafez and Gupta [12], where it was shown that the supersonic swirl number (air only, no fuel injection) decays from 0.36 at nozzle exit to about 0.07 at $z/D = 1.25$. At low M_{rel}, on the other hand, Fig. 14 shows that a mixing enhancement of only 2% is observed at z/D of 0.1 that increases to 9% at z/D of 1.25. The previously mentioned effects of M_{rel} and shear angle explain this behavior. Also recall that no swirl was imparted to the injected fuel simulant, which suggests that decreasing M_{rel} will further aid the decay of supersonic swirl number; a trend that was reported in [26]. The reduced swirl number at low M_{rel} thus further explains the deteriorated mixing at low M_{rel}.

The effect of swirl is also noticed in the distributions of the centerline Mach number in Fig. 12. Swirl induces a slight increase in centerline Mach number, which is believed to be attributed to swirl-induced mixing enhancement as well. Recall that helium was used as fuel simulant, and the speed of sound in helium is three times that in air. Therefore, better mixing yields a lower centerline speed of sound in the helium-rich core flow, which explains the increase in Mach number. Such increase induces an upstream shift in the axial location of core-flow throat, as observed in Fig. 13. Based on the aforementioned analysis of shear angle, this shift in core-flow throat is expected to adversely affect mixing, which is indeed true. The earlier transition to positive shear angle propagation further explains why the swirl-induced mixing enhancement is significant at low z/D and diminishes as the flow progresses further downstream.

D. Effect of Air–Fuel Density Ratio

Having analyzed the effect of relative Mach number, the analysis proceeds to examine the effect of air–fuel DR at constant M_{rel}. DR is defined here as the ratio of throat density of air to injection density of fuel. Also recall that the close values of sonic air velocity under

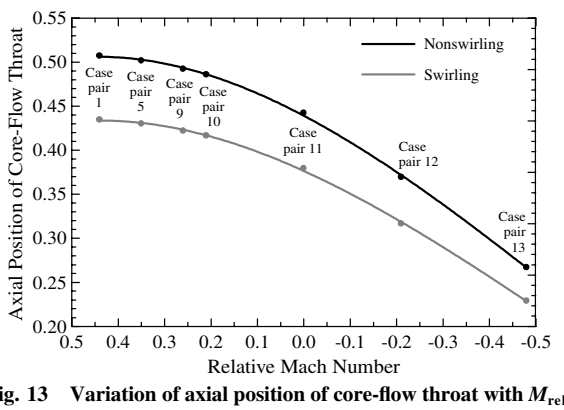

Fig. 13 Variation of axial position of core-flow throat with M_{rel}.

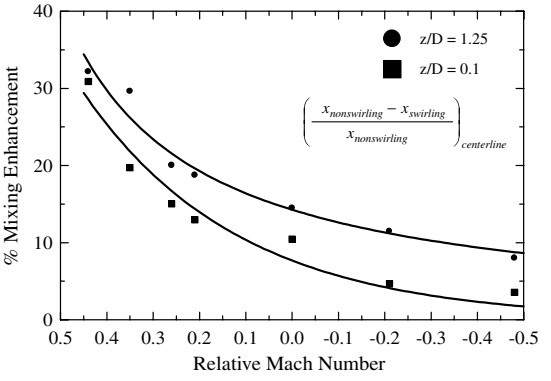

Fig. 14 Variation of percentage swirl-induced mixing enhancement with M_{rel} at different axial positions.

nonswirling and swirling conditions allowed for examining the same values of DR with and without swirl. Another very important detail to be pointed out again is that swirl is imparted to air at matched mass flow; that is, all swirling cases have the same mass flow rate of the nonswirling ones (175 g/s). This implies that the swirling cases have the elevated nozzle reservoir pressure of 8.82 bar.

Keeping all airflow properties constant, fuel was simulated by different inert-gas mixtures (helium, argon, and krypton). The mixture composition is varied to change mixture density and, consequently, DR. To maintain a constant M_{rel} of 0.21 throughout this analysis, the injection velocity was adjusted to account for the changes in a_{fuel} due to the varying injectant composition. The supply pressure of fuel was carefully selected for each case pair to match the total pressures of fuel and air at injection. Compressible injection is used throughout this analysis, except for case pair 14, which is the same as case pair 10 from the M_{rel} analysis. Case pair 23 represents the extreme conditions, where fuel is injected at its sonic velocity; that is, the injection system is choked.

Figure 15 shows the effect of DR at constant M_{rel}. The experimental results (Mie-scattering images) are depicted in Fig. 15a, while Fig. 15b shows the numerical results in the form of fuel-mixture-fraction profiles. The nonswirling cases are depicted in the top row, while the bottom row contains the swirling cases. The values of DR and injection Mach number of each case pair are indicated at the top of each column, together with the composition of fuel simulant.

In light of the comprehensive M_{rel} analysis, the effect of DR will be analyzed here in a concise fashion. It can be observed from Fig. 15 that the air–fuel shear layer again initiates with a negative angle that transforms later to positive. Consequently, the cross-sectional area of core flow converges initially to a throat before propagating divergently. This allows the core flow to accelerate from the subsonic Mach numbers of injection to supersonic maxima of 1.84–2.13 in Fig. 16. The variation of axial position of core throat with DR is shown in Fig. 17. Notice that at high DR, the core flow propagates axially for about 0.5D with a negative-shear angle. However, at a DR of 2.29, the throat of the core flow is exactly at the nozzle exit, and

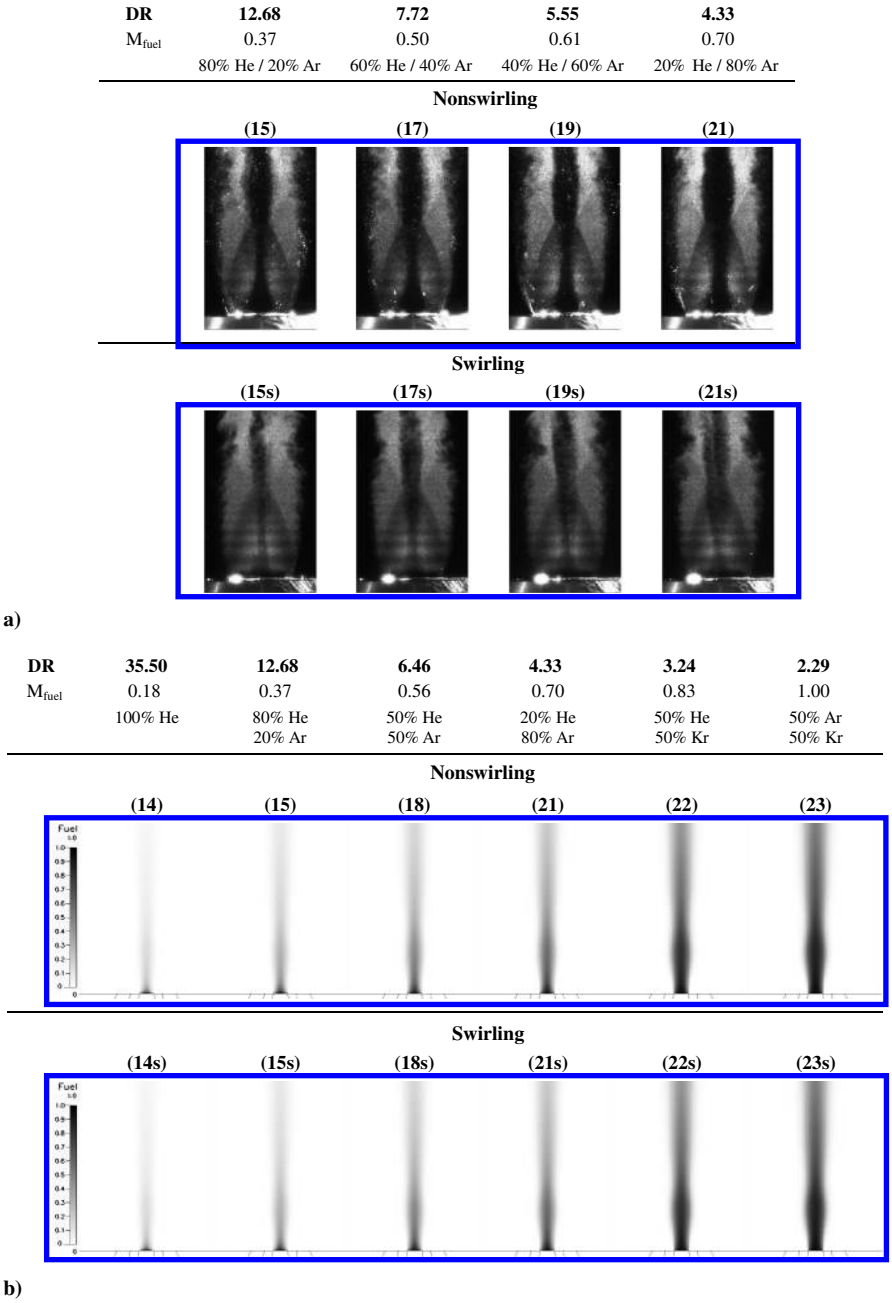

Fig. 15 Effects of DR at constant M_{rel} of 0.21: a) Mie-scattering images and b) numerical results (fuel mass fraction profiles).

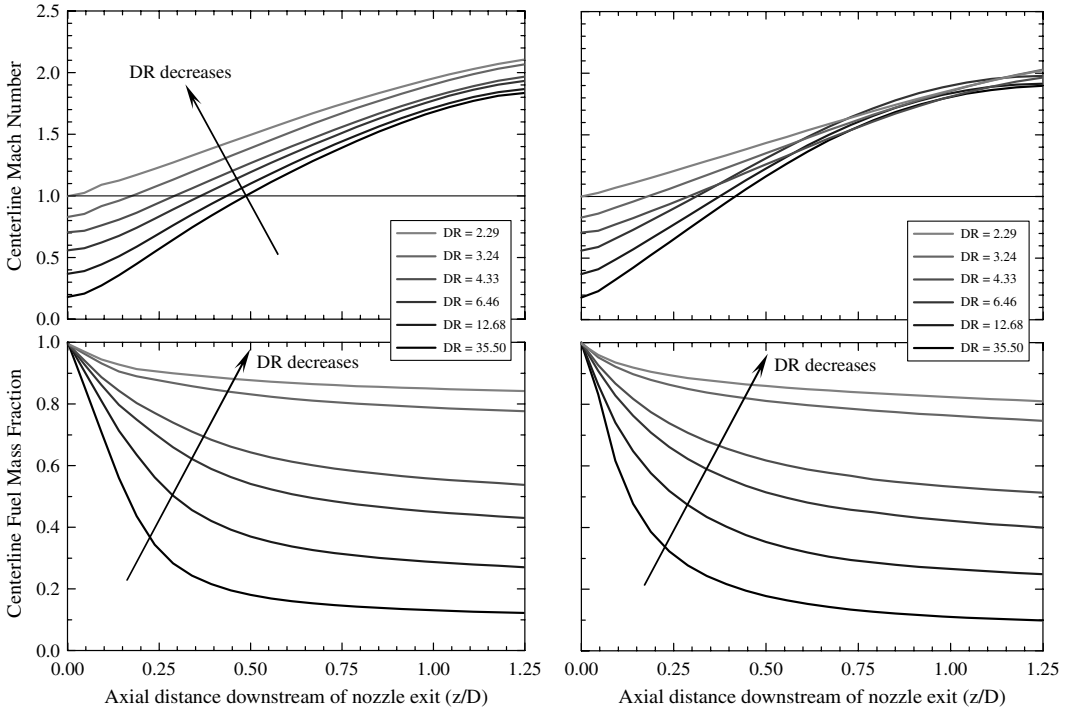

Fig. 16 Axial variations of centerline Mach number and fuel mass fraction for different values of DR under nonswirling (left) and swirling (right) conditions.

negative-shear-angle propagation is completely absent. Also notice from the rate of decay in the centerline fuel mass fraction in Fig. 16 that a fully supersonic, positive-angled shear layer (DR = 2.29) yields deteriorated mixedness as compared with the supersonic/subsonic negative-angled shear layer at DR = 35.50. The findings of Figs. 16 and 17 are confirmed in the Mie-scattering images of Fig. 15, where mixing is observed to deteriorate gradually as DR is decreased, as evidenced from the increase in size of unseeded fuel-rich core flow.

Similar to the analysis of M_{rel}, the analysis of DR is concluded here by highlighting the effect of swirl. The first outcome of applying swirl is significant mixing enhancement, which can be clearly observed from the Mie-scattering images in Fig. 15. Notice that the unseeded core flow in all swirling cases has considerably brighter shades and smaller sizes. Enhanced mixing with the surrounding supersonic airflow explains the presence of seeding particles inside the core flow of swirling cases, whereas the fuel-rich core flows of nonswirling cases are particle free.

The positive effect of swirl on mixing is also confirmed in Fig. 16. It can be seen that swirl induces an overall reduction in centerline fuel mass fraction, regardless of DR, which suggests better mixing. Once more it can be observed that the effect of swirl is significant at low z/D and fades as the flow progresses further downstream. Figure 18 compares the percentage swirl-induced mixing enhancement at z/D of 0.1 and 1.25 over the examined range of DR. At high DR, mixing is enhanced by about 13% after $0.1D$ of flow travel and an additional 6% over only the axial spans of $0.1D$ to $1.25D$. This can again be explained by the decaying supersonic swirl number. At low DR, on the other hand, Fig. 18 shows that a mixing enhancement of only 1% is observed at z/D of 0.1 that increases to 4% at z/D of 1.25. The aforementioned effects of DR and shear angle explain such behavior. Also recall that no swirl was imparted to the injected fuel simulant, which suggests that decrease in DR will further aid the decay of supersonic swirl number: a trend that was also reported in [26]. The reduced swirl number at low DR thus further explains the deteriorated mixing with decrease in DR.

The effect of swirl is also noticed in the distributions of centerline Mach number shown in Fig. 16. It should be noticed, however, that, unlike the M_{rel} analysis, swirl does not just induce an increase in centerline Mach number for all examined DR. For ratios greater than about 4.3, swirl induces a slight increase in Mach number, but for DR smaller than 4.3 (i.e., case pairs 22 and 23), the centerline Mach number distributions actually undergo a slight reduction due to swirl. In spite of the different M_{rel} and DR behaviors, the latter is still believed to be attributed to swirl-induced mixing enhancement as well. Recall that mixtures of helium, argon, and krypton were used as fuel simulants. The speeds of sound in such simulants are higher than that in air for case pairs 14–20 with DR > 4.3. Case pair 21 has a DR of 4.33 and a speed of sound almost equal to that of air, while case pairs 22 and 23 have DR < 4.3 with lower speeds of sound. Therefore, better mixing due to swirl is expected to yield lower centerline speeds of sound in the fuel-rich core flows of case pairs 14–20, no significant change in case pair 21, but higher centerline speeds of sound in case pairs 22 and 23. This explains the nonuniform effect of swirl on Mach number observed in Fig. 16. Swirl induces an upstream shift in the axial location of core-flow throat in case pairs 14, 15, and 18, as observed in Fig. 17, but results in a slight downstream shift in case pair 22. Case pair 21 experiences no significant change, and case pair 23 is already unique in the sense that sonic injection is implemented with a fuel-simulant speed of sound much smaller than that of air. Consequently, the injection velocity is much lower than the sonic velocity of air, which makes air the high-speed side of the air–fuel shear layer. The throat of fuel-rich

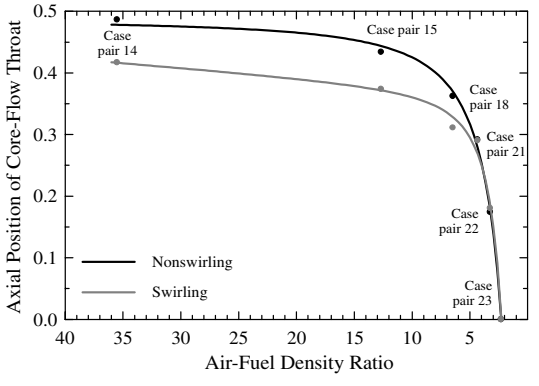

Fig. 17 Variation of axial position of core-flow throat with DR.

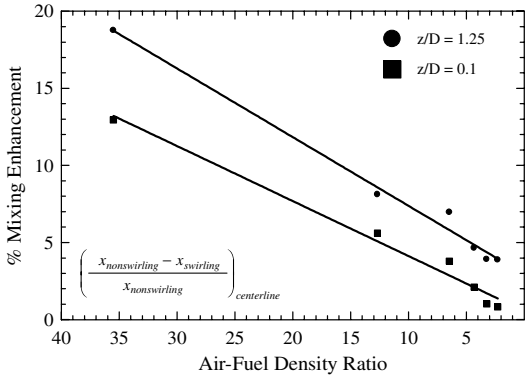

Fig. 18 Variation of percentage swirl-induced mixing enhancement with DR at different axial positions.

core flow can, therefore, never be shifted downstream, as this would mean that the core-flow velocity decreases after injection, while that of the expanding supersonic airflow increases.

E. Mixing-Layer Growth

The analysis of the effect of swirl is concluded here by examining how swirl affects the thickness and growth of the compressible mixing layer. Similar to our previous study [12], where the pitot thickness δ_{pit} was quantified at multiple values of convective Mach number, the mixture-fraction-based thickness δ_x is examined here, highlighting the effect of swirl. The reader is referred to the work of Papamoschou and Roshko [27] for a complete description of the pitot thickness and the convective frame of reference.

The variable δ_x is defined here as the width of the fuel-mixture-fraction profile x from 0.05 to 0.95. The analysis of δ_x is carried out on all the numerical cases given in Table 1, since their simulations contain all the necessary data. The axial positions $z/D = 0.1$ and 1.0 were selected in each case. Twenty-four additional simulations were conducted to replicate the 12 numerical case pairs of Table 1 under incompressible conditions, while maintaining their individual velocity and DRs. The incompressible values of δ_x were thus obtained, and the normalized δ_x (i.e., ratios of compressible to incompressible values) were finally calculated. Figure 19 is the fruit of this effort, where the normalized values of δ_x are plotted versus the airside convective Mach number. All data points fall in the Mach number range 0.25–0.83. The pitot-thickness data points of Papamoschou and Roshko are also included.

Two important conclusions can be made from Fig. 19. First, the δ_{pit} and δ_x thicknesses of the mixing layer are comparable, which is true from the direct comparison in Fig. 19 as well as from the comparison of the present findings to those of our previous study [12]. This also agrees with the concentration-thickness data reported in Naughton et al. [11]. The second conclusion to be made from Fig. 19 is that the normalized δ_x decreases with the application of swirl. The dimensional (i.e., non-normalized) δ_x, on the other hand, was observed to actually increase slightly with swirl, which again agrees with the findings our previous study as well as those of Naughton et al., where it was shown that the positive effect of swirl increases with compressibility, although the dimensional growth rates are still less than those of their incompressible counterparts. This behavior was also confirmed by Cutler et al. [28], Cutler and Levey [29], and Levey [30].

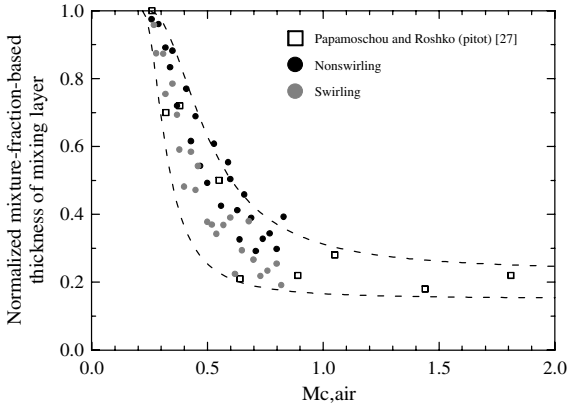

Fig. 19 Normalized mixture-fraction-based thickness δ_x of mixing layer versus airside convective Mach number $M_{c,\text{air}}$.

VI. Conclusions

This experimental/numerical work examined the effect of imparting swirl to underexpanded nozzle airflow on supersonic mixing. Matched mass flow conditions were considered. A convergent nozzle with swirling capabilities was used to generate the underexpanded airflow. Fuel was injected coaxially at the nozzle throat. Nonreacting conditions were considered, wherein fuel was simulated by mixtures of helium, argon, and krypton inert gases. Analyses were made of the effects of relative Mach number and DR across air–fuel shear layer. The effects of these parameters on mixing were investigated under both nonswirling and swirling conditions. It was concluded that the positive effect of swirl on supersonic mixing is noticeable, even at the low degree of swirl examined here. Better mixing was observed between the supersonic and subsonic parts of the diamond-shock air flowfield at no fuel injection, as well as between the supersonic air and the subsonic injected fuel. The compressible mixing-layer thickness was found to increase slightly with swirl. However, when normalized to its incompressible counterpart, the compressible thickness was observed to decrease with swirl, because the former increases more with swirl than the latter. Decreasing the air–fuel relative Mach number and/or DR was found to deteriorate mixing. On the other hand, decreasing the compressibility of the injected fuel (i.e., injecting fuel at lower subsonic Mach numbers) improves mixing. The cross-sectional area of fuel-rich core flow has to converge first before this core flow reaches a throat, after which it propagates supersonically. This behavior was found to be advantageous, as it results in better mixing.

Acknowledgments

This work was supported by the Space Vehicle Technology Institute, jointly funded by NASA, the Department of Defense, and the U.S. Air Force, within the NASA Constellation University Institutes Project, with Claudia Meyer as the Project Manager. This support is gratefully acknowledged. The simulation packages CFD-GEOM, CFD-FASTRAN, and CFD-VIEW were provided by ESI Group and CFD Research Corporation. This support is gratefully acknowledged. Help and support provided by Kenneth H. Yu, University of Maryland, with the design of the Mie-scattering setup, is greatly appreciated. The assistance provided by Adam Kareem in data acquisition is also appreciated.

References

[1] Buckley, P. L., Craig, R. R., Davis, D. L., and Schwartzkopf, K. G., "The Design and Combustion Performance of Practical Swirlers for Integral Rocket/Ramjets," *AIAA Journal*, Vol. 21, No. 5, 1983, pp. 733–740.
doi:10.2514/3.8141

[2] Swithenbank, J., and Chigier, N. A., "Vortex Mixing for Supersonic Combustion," *12th Symposium (International) on Combustion*, The Combustion Inst., Pittsburgh, PA, 1969, pp. 1153–1162.

[3] Cutler, A. D., and Doerner, S. E., "Effects of Swirl and Skew upon Supersonic Wall Jet in Crossflow," *Journal of Propulsion and Power*, Vol. 17, No. 6, Nov.–Dec. 2001, pp. 1327–1332.
doi:10.2514/2.5882

[4] Kraus, D. K., "An Experimental Investigation of Mixing Enhancement in a Simulated Scramjet Combustor by Use of Swirling Jets," M.Sc. Thesis, School of Engineering and Applied Science, George Washington Univ., Washington, D. C., Aug. 1993.

[5] Kraus, D. K., and Cutler, A. D., "Mixing of Swirling Jets in a Supersonic Duct Flow," *Journal of Propulsion and Power*, Vol. 12, No. 1, Jan.–Feb. 1996, pp. 170–177.
doi:10.2514/3.24007

[6] Cutler, A. D., Levey, B. S., and Kraus, D. K., "Near-Field Flow of Supersonic Swirling Jets," *AIAA Journal*, Vol. 33, No. 5, May 1995, pp. 876–881. doi:10.2514/3.12362
[7] Yamasaki, H., Okuno, Y., Torii, S., Masuda, J., Tsutsumi, M., Oda, N., Uchiyama, K., Kouka, H., Fujimoto, T., Suzuki, H., and Suzuki, M., "Improvement of Disk MHD Generator Performance by Inlet Swirl," 30th Plasmadynamics and Lasers Conference, Norfolk, VA, AIAA Paper 1999-3658, 1999.
[8] Kitamura, E., Matsumoto, M., Koike, S., and Masuya, G., "PIV Measurement of Supersonic Swirling Jet," *Journal of the Visualization Society of Japan*, Vol. 22, No. 1, 2002, pp. 189–192.
[9] Yaguchi, H., Suzuki, K., Takita, K., and Masuya, G., "Mixing Enhancement of Supersonic Jet with Swirl," *Nippon Kikai Gakkai Ryutai Kogaku Bumon Koenkai Koen*, Vol. 78, No. 1, 2000, pp. 101–104.
[10] Settles, G. S., "Supersonic Mixing Enhancement by Vorticity for High-Speed Propulsion," NASA CR 188920, Oct. 1991.
[11] Naughton, J. W., Cattafesta, L. N., and Settles, G. S., "An Experimental Study of Compressible Turbulent Mixing Enhancement in Swirling Jets," *Journal of Fluid Mechanics*, Vol. 330, 1997, pp. 271–305. doi:10.1017/S0022112096003679
[12] Abdelhafez, A., and Gupta, A. K., "Effect of Swirl on Shock Structure in Underexpanded Supersonic Airflow," *Journal of Propulsion and Power*, Vol. 26, No. 2, 2010, pp. 215–229. doi:10.2514/1.45716
[13] Murakami, E., and Papamoschou, D., "Experiments on Mixing Enhancement in Dual-Stream Jets," 39th AIAA Aerospace Sciences Meeting and Exhibit, Reno, NV, AIAA Paper 2001-0668, 2001.
[14] Carpenter, P. W., "A Linearized Theory for Swirling Supersonic Jets and its Application to Shock-Cell Noise," *AIAA Journal*, Vol. 23, No. 12, 1985, pp. 1902–1909. doi:10.2514/3.9194
[15] Yu, Y. K., Chen, R. H., and Chew, L., "Screech Tone Noise and Mode Switching in Supersonic Swirling Jets," *AIAA Journal*, Vol. 36, No. 11, 1998, pp. 1968–1974. doi:10.2514/2.323
[16] Yu, Y. K., "An Experimental Study of Underexpanded Supersonic Swirling Jets," Ph.D. Thesis, Univ. of Central Florida, Orlando, FL, Dec. 1997.
[17] Gupta, A. K., Lilley, D. G., and Syred, N., "Swirl Flows," Abacus Press, Preston, Lancashire, U. K.,1984.
[18] Linck, M., "Spray Flame and Exhaust Jet Characteristics of a Pressurized Swirl Combustor," Ph.D. Thesis, Univ. of Maryland, College Park, MD, May 2006.
[19] Abdelhafez, A., and Gupta, A. K., "Swirling Airflow through a Nozzle: Choking Criteria," *Journal of Propulsion and Power*, Vol. 26, No. 4, 2010, pp. 754–764. doi:10.2514/1.47956
[20] Yakhot, V., Orszag, S. A., Thangam, S., Gatski, T. B., and Speziale, C. G., "Development of Turbulence Models for Shear Flows by a Double Expansion Technique," *Physics of Fluids A*, Vol. 4, No. 7, 1992, pp. 1510–1520. doi:10.1063/1.858424
[21] Baldwin, B. S., and Lomax, H., "Thin Layer Approximation and Algebraic Model for Separated Turbulent Flows," 16th AIAA Aerospace Sciences Meeting, Huntsville, AL, AIAA Paper 1978-257, 1978.
[22] Abdelhafez, A., and Gupta, A. K., "Numerical Investigation of Oblique Fuel Injection in a Supersonic Combustor," 46th AIAA Aerospace Sciences Meeting, Reno, NV, AIAA Paper 2008-0068, 2008.
[23] Abdelhafez, A., Gupta, A. K., Balar, R., and Yu, K. H., "Evaluation of Oblique and Traverse Fuel Injection in a Supersonic Combustor," 43rd AIAA/ASME/SAE/ASEE Joint Propulsion Conference & Exhibit, Cincinnati, OH, AIAA Paper 2007-5026, 2007.
[24] Courant, R., Friedrichs, K., and Lewy, H., "On the Partial Difference Equations of Mathematical Physics," *IBM Journal of Research and Development*, Vol. 11, No. 2, March 1967, pp. 215–234. doi:10.1147/rd.112.0215
[25] Claypole, T. C., and Syred, N., "The Effects of Swirl Burner Aerodynamics on NOx Formation," *Proceedings of 18th Symposium (International) on Combustion*, Combustion Inst., Pittsburgh, PA, 1981, pp. 81–89.
[26] Abdelhafez, A., and Gupta, A. K., "Swirl Effects on Free Underexpanded Supersonic Airflow," 47th AIAA Aerospace Sciences Meeting and Exhibit, Orlando, FL, AIAA Paper 2009-1557, 2009.
[27] Papamoschou, D., and Roshko, A., "The Compressible Turbulent Shear Layer: An Experimental Study," *Journal of Fluid Mechanics*, Vol. 197, 1988, pp. 453–477. doi:10.1017/S0022112088003325
[28] Cutler, A. D., Levey, B. S., and Kraus, D. K., "An Experimental Investigation of Supersonic Swirling Jets," 24th AIAA Fluid Dynamics Conference, Orlando, FL, AIAA Paper 1993-2922, 1993.
[29] Cutler, A. D., and Levey, B. S., "Vortex Breakdown in a Supersonic Jet," AIAA Paper 1991-1815, June 1991.
[30] Levey, B. S., "An Experimental Investigation of Supersonic Vortical Flow," M.S. Thesis, School of Engineering and Applied Science, George Washington Univ., Washington, D. C., Sept. 1991.

R. Bowersox
Associate Editor